ACS APPLIED MATERIALS & INTERFACES

Research Article

www.acsami.org

Micropatterned Coumarin Polyester Thin Films Direct Neurite Orientation

Aleesha M. McCormick,[†] Murthy V. S. N. Maddipatla,[‡] Shuojia Shi,[§] Elaheh A. Chamsaz,[‡] Hiroshi Yokoyama,[§] Abraham Joy,*[,‡] and Nic D. Leipzig*[,†]

[†]Chemical and Biomolecular Engineering and [‡]Department of Polymer Science, The University of Akron, Akron, Ohio 44325, United States

[§]Liquid Crystal Institute, Kent State University, Kent, Ohio 44240, United States

Supporting Information

ABSTRACT: Guidance and migration of cells in the nervous system is imperative for proper development, maturation, and regeneration. In the peripheral nervous system (PNS), it is challenging for axons to bridge critical-sized injury defects to achieve repair and the central nervous system (CNS) has a very limited ability to regenerate after injury because of its innate injury response. The photoreactivity of the coumarin polyester used in this study enables efficient micropatterning using a custom digital micromirror device (DMD) and has been previously shown to be biodegradable, making these thin films ideal for cell guidance substrates with potential for future in vivo applications. With DMD, we fabricated coumarin polyester thin films into 10 × 20 μm and 15 × 50 μm micropatterns with depths ranging from 15 to 20 nm to enhance nervous system cell alignment. Adult primary neurons, oligodendrocytes, and astrocytes were isolated from rat brain tissue and seeded onto the polymer surfaces. After 24 h, cell type and neurite alignment were analyzed using phase contrast and fluorescence imaging. There was a significant difference ($p < 0.0001$) in cell process distribution for both emergence angle (from the body of the cell) and orientation angle (at the tip of the growth cone) confirming alignment on patterned surfaces compared to control substrates (unpatterned polymer and glass surfaces). The expected frequency distribution for parallel alignment (≤15°) is 14% and the two micropatterned groups ranged from 42 to 49% alignment for emergence and orientation angle measurements, where the control groups range from 12 to 22% for parallel alignment. Despite depths being 15 to 20 nm, cell processes could sense these topographical changes and preferred to align to certain features of the micropatterns like the plateau/channel interface. As a result this initial study in utilizing these new DMD micropatterned coumarin polyester thin films has proven beneficial as an axon guidance platform for future nervous system regenerative strategies.

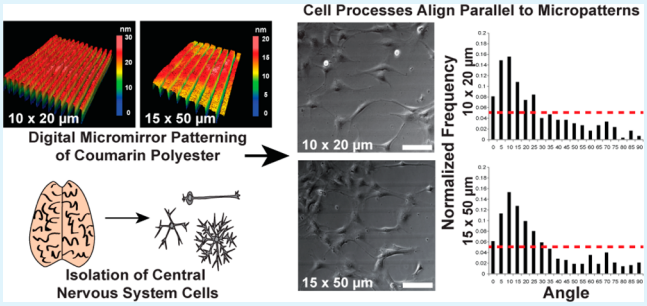

KEYWORDS: *Axon guidance, nervous system regeneration, micropatterned polymers, photoreactive polymers, nanotopography, cortical neurons, glial cells*

1. INTRODUCTION

Trauma to the nervous system typically results in a lengthy recovery with uncertain regeneration. The peripheral nervous system (PNS) is known to regenerate slowly at about 2−4 mm/day;[1] however, injury resulting in a critical-sized defect (>3 cm in humans (for review, see refs 2 and 3)) generally results in slow or incomplete nerve reinnervation. Currently, nerve grafts and nerve guidance conduits (NGCs) are clinically used to bridge critical-sized defects in the PNS. These conduits have shown degrees of success in humans as well as animal models; however, an agreed upon approach has yet to be formulated that would result in fully functional PNS nerve regeneration.[2] Additionally, the central nervous system (CNS) rarely exhibits regeneration after injury because of several intrinsic barriers.[4] This additional hurdle has proven difficult to overcome in creating successful nerve guidance/regeneration approaches. In response, biomaterial based platforms that stimulate the regeneration of a fully functional nerve are under development.[5,6] In these models it is important to provide similar cues and processes that guide nervous system development and regeneration to overcome native obstacles that occur during injury.

Neural networks are the central processing units that enable complex neuronal functions and are formed when neurites reach their synaptic targets. The growth cone on the tip of these neurites begins the process of synaptogenesis as it encounters, interprets and transduces extracellular cues from a host of inputs including biomolecular, electrical, topographical

Received: July 7, 2014
Accepted: October 27, 2014
Published: October 27, 2014

and mechanical signals (for reviews, see refs 7−10). These cues are vital to the initiation and extension of neurites as well as the migration of cells, ultimately resulting in the formation and development of the mature nervous system. In particular, contact guidance from topographical cues has been shown to play a crucial role during retinal and optic stalk development as seen in embryonic mice and chickens.[11,12] Neurons have a close relationship with glia, the supportive cells of the nervous system, and rely heavily on their physical (e.g., morphology) and chemical signals for guidance and migration during development and regeneration (for review, see ref 13). One of the first descriptions of the phenomenon of topographical cell guidance occurred a century ago.[14] Today new technologies are enabling increasingly complex topographical cues to be integrated into biomaterial platforms, which facilitate enhanced and more precise control of neuronal extension and repair.

NGCs have been utilized for decades as a bridge for nervous system repair, and the gold standard to overcome these critical-sized defects has been autografts. Alternatively, NGCs fabricated from synthetic or natural polymers are also used clinically, especially in cases where autografts are not an option. There are four bioresorbable FDA-approved NGCs synthesized from either polyglycolic acid (PGA) or poly-D,L-lactide-*co*-caprolactone (PLCL) and two fabricated from type I collagen, which degrade on the order of 3 months to 4 years.[15] One nonresorbable NGC made from poly(vinyl alcohol) (PVA) has also been approved.[15] However, autografts and the current hollow NGCs do not provide functional recovery in all instances of nerve injury. As a result research has been geared toward other biopolymers and synthetic materials that contain specific characteristics that mimic beneficial cues from native tissue for optimal recovery. Rutkowski et al.[16] fabricated PLA NGCs using a transfer technique where silicon wafers containing micropatterns were formed with reactive ion etching, followed by PVA casting onto the pattern, and finally PLA was spun onto the substrate and released by dissolving the PVA in water. The final PLA films contained 10 μm channels and 10 μm plateaus, with a depth of 4.3 μm, and were wrapped into NGCs. These micropatterned tubes encouraged axon outgrowth but did not significantly enhance regeneration of a 10 mm rat sciatic nerve compared to a tube without microchannels; however, the addition of Schwann cell to the NGC did increase functional recovery in the animals. Therefore, an increase in neurite alignment to microchannels can be achieved through a combination of topographical, chemical and biological cues.[17,18] Additionally, hollow NGCs modified with intraluminal fibers, channels, microchannels and biomolecular or peptide surface modifications have been proposed as alternative strategies to align and guide axons toward their target.[19]

Popular biodegradable and nonbiodegradable substrates such as poly(methyl methacrylate) (PMMA), polystyrene (PS), polydimethylsiloxane (PDMS), poly(L-lactic acid) (PLLA), polycaprolactone (PCL), poly(D,L-lactic acid) (PLA), poly-(lactic-*co*-glycolic-acid) (PLGA), quartz, and silicon have been used to make various topographical cues to encourage cell adhesion, alignment, and differentiation (for review, see refs 20 and 21). Fabrication methods typically rely on lithography techniques utilizing some combination of chemicals, light, electrons, ions, molds, masks, or imprints for the formation of structures, such as micro- and nanoscaled channels, pillars, pits, steps, etc. (for reviews, see ref 20−22). Cell type and substrate dimensions are important factors that determine cell alignment, neurite extension, and process orientation responses. For example, neuron-like PC12 cells have been shown to align to channels ranging in width from 20 to 60 μm with 10 μm wide plateaus and a depth of 11 μm; however, parallel neurite alignment was significantly enhanced in 20, 30, and 40 μm channels.[23] Dorsal root ganglia (DRG) have been shown to align to larger channel features ranging from 100 to 250 μm, while 100 μm wide channels decrease neurite branching and significantly increase primary neurite length compared to the other width dimensions.[24] The typical diameter of a neuron ranges from 10 to 20 μm[25] with axon caliber varying from 1 to 20 μm.[26] Therefore, it is important to consider how various feature sizes elicit a specific cellular response, such as neuronal branching, length, number, and polarity. These various responses determine the appropriate topographical dimensions, such as channel width and depth, for a specific cell/tissue application. Materials with well aligned micropatterns may be useful in applications, such as central or peripheral nerve repair, especially when incorporated into conduit based strategies as mentioned above. To realize such applications, the use of degradable materials is preferred and it is critical that the fabrication of such patterned surfaces is both precise and efficient, presented at the length scales at which neurons can sense and respond.

We recently reported the synthesis and characterization of a photoreactive polyester in which coumarin units are incorporated along the polymer backbone.[27] This design enables the polymer to demonstrate dual photoreactive properties. Irradiation at 350-365 nm results in polymer chain cross-linking as a result of a [2 + 2] cycloaddition reaction between the coumarin units. At 254 nm, the polymer undergoes chain scission reactions at the ester bonds. We also utilized this dual photochemical property to fabricate micron sized features on polymer thin film coatings. Furthermore, we have also shown that incubation of solvent cast films of these polymers (70 μm thickness) in PBS over a 2 month period results in hydrolytic degradation of the coumarin polyester film.

Since the coumarin polyester described above is also biodegradable, it is conceivable that such photoreactive and biodegradable materials could be used to fabricate micropatterned NGCs, in which the micropatterns will provide contact guidance for cells and the patterned NGC will degrade once nerve regeneration has occurred. This study is an evaluation of that hypothesis, wherein we aim to demonstrate the generation of micropatterns over a large area (2.5 × 2.5 cm) with a maskless optical pattern generator using a digital micromirror device (DMD). The working principle of the DMD is similar to the commercial digital light processing (DLP) projector, except that the magnifying projection lens is replaced with a high quality demagnifying lens system. A computer generated pattern data is transferred to the DMD and converted to an on−off pattern of micromirrors.[28] Upon demagnification, the depth of focus becomes extremely small even below a submicron range when the numerical aperture of the final objective is higher than 0.2. The current system is capable of autofocusing using a red LED light, to which the materials are insensitive, with the DMD as the confocal aperture. This feature allows a fully automated operation, thereby allowing a sequential exposure of numerous patterns.[29]

We further characterize the generated patterns and evaluate the guidance of cortical neuronal cells within the micropatterned surface. The use of the DMD can rapidly generate micropatterns over a large area, thus, the combination of rapid

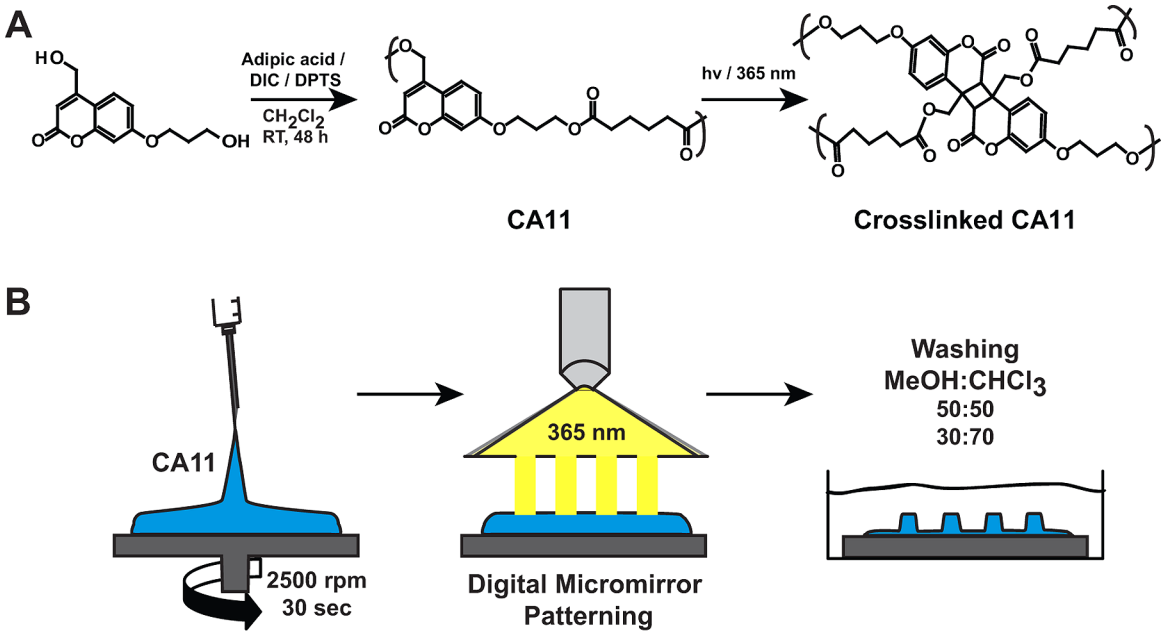

Figure 1. (A) Synthesis and cross-linking reaction of coumarin polyester (CA11). (B) CA11 was spun onto substrates and allowed to dry. Digital patterns (10 × 30 μm and 10 × 60 μm) were designed and a DMD focused these patterns onto the CA11 polymer. The regions exposed to the light (365 nm) cross-linked the polymer, whereas areas that were not exposed to light were washed away during two different mixture of methanol (MeOH) and chloroform ($CHCl_3$) washes to form the microchannels.

prototyping and the use of this photodegradable and biodegradable polyester provides a potentially transformative method for the generation of NGCs, as well as other implants for cell guidance. Other materials used as NGCs seldom combine all three of these advantages.

The primary objective of this study was to demonstrate that this technique can create micropatterned biodegradable polymers that guide and align adult neurons from a mixed cortical cell population (primarily neurons in addition to astrocytes and oligodendrocytes) isolated from adult rat brain tissue. On the basis of preliminary work, we hypothesize that these cells will align parallel with the polymer channels compared to a control polymer surface made of the same material with no channels and an additional control glass substrate. Microscopy and immunohistochemical methods were used to analyze neurite alignment, as well as to detect the cell populations present. Future endeavors will focus on analyzing other cell types on these topographies in addition to fine-tuning the depth and width dimensions for optimal cell alignment and extension for translation into a clinically relevant animal nerve guidance model.

2. MATERIALS AND METHODS

2.1. Synthesis of Coumarin Polyester CA11. The synthesis of the monomers and polymer has been described in our earlier publication.[27] In brief, the coumarin polyester CA11 (Figure 1A) is synthesized by the carbodiimide mediated polymerization of the coumarin diol (250 mg, 1 mmol, 1 equiv) with adipic acid (146 mg, 1 mmol, 1 equiv). The above diol and diacid are taken in an evacuated and N_2 filled round bottomed flask along with 4-(*N*,*N*-dimethylamino)pyridinium-4-toluenesulfonate (DPTS, 117 mg, 0.4 mmol, 0.25 equiv) and *N*,*N*-diisopropylcarbodiimide (DIC, 470 mL, 3 mmol, 3 equiv). The reaction was carried out in CH_2Cl_2 at RT for 48 h. The polymer was precipitated in a mixture of alcohols (MeOH/EtOH/iPrOH 1:1:1). The polymer was collected, centrifuged and dried under vacuum to yield a white solid (310 mg, 85%). ^{1}H NMR (300 MHz, $CDCl_3$): δ, ppm 1.68−1.78 (m, 4H) 2.17−2.18 (m, 2H), 2.35−2.38 (m, 2H), 2.49−2.51 (m, 2H), 4.12(m, 2H), 4.28−4.30 (m, 2H), 5.28(m, 2H), 6.31 (s, 1H), 6.84−6.88 (br, 2H), 7.40−7.43 (d, 1H).

2.1.1. Materials. Adipic acid and solvents were purchased from Fisher Scientific or VWR. Diisopropyl carbodiimide (DIC) was purchased from Oakwood Chemicals.

2.1.2. NMR Spectroscopy. ^{1}H NMR spectra were recorded on a Varian Mercury 300 MHz or Varian 500 MHz spectrometer (Palo Alto, CA, USA). Chemical shifts were recorded in ppm (δ) relative to TMS.

2.1.3. SEC Analysis. Size exclusion chromatography (SEC) was performed to determine polymer Mn and Mw using a TOSOH EcoSEC HLC-8320 instrument equipped with two TSK-GEL Super H 3000 columns and one TSK-GEL Super H 4000 column in series running $CHCl_3$. Molecular weights were obtained relative to PS standards.

2.2. Micropatterning of the Photodegradable Polymer. The polymer (CA11) was precipitated from iPrOH−EtOH−MeOH (1:1:1) at least 3 times to remove oligomers and the urea byproduct. The photodegradable polymer was dissolved in chloroform (2 wt % solution) for 18 h and filtered using 0.45 μm PTFE filter. Coverslips (12 mm) were soaked in alcoholic KOH solution for 2 h, washed with deionized water several times and dried in a vacuum oven. The polymer solution was spin coated on the coverslips (2500 rpm, 30 s) and dried (Figure 1B). The DMD used consists of 1024 × 768 array of independently switchable 13.7 × 13.7 μm micromirrors (Discovery 4100, Digital Light Innovations, Texas Instruments). Digital patterns were made with specific dimensions (10 μm channel × 30 μm plateau or 10 μm channel × 60 μm plateau), by Inkscape, an open source vector graphics editor program. These digital patterns were focused onto the polymer-coated coverslips without a mask and exposed to light (USHIO (Discharge) Super High Pressure Mercury lamp (major peaks 365, 405, 436 nm); USH-350D) for 7 min causing CA11 to cross-link in the regions exposed to the light (Figure 1). The microchannels were revealed by processing the irradiated coverslips in a mixture of methanol and chloroform (solvent gradient MeOH/$CHCl_3$ 50:50 to 30:70) by immersing them in this solution for 7 min followed by a rinse of 1−2 pipet washes of the fresh 50:50 solvent and 1−2 pipet washes with 30:70 MeOH/$CHCl_3$ (Figure 1B). These coverslips with micropatterned surfaces were sealed in a container kept

at 4 °C to prevent degradation. 2D images were obtained using a fluorescent microscope (Olympus IX81, Tokyo, Japan) with a DAPI filter and an Alicona infinite focus microscope (IFM; Bartlett, IL, USA). Analysis of the plateau widths and channel depths and widths were verified with an optical profilometer (NewView 7300 3D Optical Surface Profile, Zygo Corporation, Middlefield, CT, USA). Five separate regions of interest were measured using MetroPro version 7.7.0 OMP-0398J software to analyze the depth and width of the channels as well as the width of the plateaus. Plateaus were measured from the top edge to edge, channels were measured in the middle of one side of the plateau across the gap to the adjacent side and depth was determined from the top edge of the plateau straight down to the bottom of the channel. The measured dimensions for plateau width, channel width, and channel depth were averaged and the standard deviation was determined.

2.3. Adult Cortical Cell Isolation. Isolation and culture of primary neurons and glia from the brain of a 7 week old female Wistar rat followed procedures similar to published literature.[30] First, the brain was dissected into small pieces using a scalpel and spring scissors and transferred to HABG medium (HibernateA, 2% B27, 0.625 mM L-glutamine; all Life Technologies, Grand Island, NY, USA). This tissue along with sterile papain solution (24 mg papain (Sigma, St. Louis, MO, USA) in 12 mL of Hibernate A with 0.625 mM L-glutamine) was placed in 37 °C water bath for 5 min. Then the tissue was transferred to the papain solution and placed on nutator at 37 °C for 30 min. After digestion, tissue was transferred to 4 mL fresh HABG medium and triturated 15 times using a serological pipet. After it settled for 1 min, 4 mL of supernatant was transferred to a new tube and 4 mL fresh HABG was added to the tissue. This process was repeated two more times, but the tissue was disrupted with a 9 in. fire polished Pasteur pipet instead of a serological pipet. After each trituration 4 mL supernatant was removed and 4 mL HABG was transferred to the tissue solution. Two OptiPrep (Sigma) density gradients were made according to reported protocol[30] and 6 mL of supernatant was carefully pipetted on top of each gradient. Both gradients were centrifuged at 800 ×G for 15 min at 22 °C. For each gradient, the cellular debris along with fraction 1, containing oligodendrocytes, was carefully aspirated. Fractions 2 and 3, containing mostly neurons and some oligodendrocytes, were collected from each gradient, strained through separate 100 μm cell strainers and diluted in HABG. Fraction 4, containing microglia and astrocytes, was not collected however this fraction was difficult to distinguish from fraction 3, which resulted in a heterogeneous cell population. Both cell solutions were spun down again for 2 min at 200 ×G, supernatant discarded and resuspended in fresh HABG medium. This procedure was repeated but cells were resuspended in 5 mL culture medium (Neurobasal medium (Life Technologies), 2% B27, 1% penicillin−streptomycin (Life Technologies), 0.625 mM L-glutamine, 5 ng/mL basic fibroblast growth factor (bFGF; Peprotech, Rocky Hill, NJ, USA)), and each tube was plated in a 25 cm^2 tissue culture flask. Cells were allowed to adhere for at least 4 h and then washed in warmed HABG medium one to two times. Finally, fresh culture medium was added back to the flasks and cells were monitored and fed fresh medium every 7 days until use.

2.4. Substrate Preparation and Cell Seeding. Four separate substrates were prepared: glass, polymer, and 10 × 30 and 10 × 60 μm polymer channels, which are the digital pattern dimensions. Polymer-coated coverslips (with and without channels), were sterilized in 70% ethanol for 1 h and rinsed in PBS (Life Technologies, pH = 7.4). Laminin (Life Technologies) was then absorbed to all surfaces at 5 μg/mL for 3 h at RT. For glass surfaces, 12 mm coverslips were steam sterilized and poly-D-lysine (Sigma) was adsorbed at 50 μg/mL overnight at RT, followed by laminin adsorption at 5 μg/mL for 3 h at RT. All surfaces were rinsed in PBS, and cells were seeded at 20,000 cells/cm^2.

2.5. Cell Alignment and Immunohistochemistry Analysis. Twenty-four hours after cell seeding, live cell phase contrast images of the total cell population were taken to quantify process alignment on all surfaces. There were 16 samples for each group, and 3−5 images were taken for each coverslip. ImageJ software was used to measure the heterogeneous population of cell process alignment; 300−400 processes were measured for each group and only processes that were clearly visible and at least 50 μm in length were measured. The emergence angle (α) measured the initial process extruding from the cell body and the orientation angle (β) measured the final alignment of the last 30 μm of the cell process according to Li et al.[31] All images were taken with the channels aligned horizontally and controls were randomly oriented with the horizontal as the reference. Angles were binned in 5° increments for histograms. Cell processes were considered parallel if ≤15° and perpendicular if they were ≥75°.[31]

For immunohistochemistry (IHC), samples were fixed in 3.7% paraformaldehyde for 10 min, rinsed with PBS (pH = 7.4) and permeabilized with 0.1% Triton X-100 (Sigma) for 5 min. After the cells were washed with PBS (pH = 7.4), 10% goat serum (Sigma) in PBS was added to block any nonspecific antibody attachment. Samples were then washed 3 times with PBS (pH = 7.4) for 10 min each wash. The following primary antibodies and dilutions were applied and incubated overnight at 4 °C: monoclonal mouse anti-βIII tubulin (1:500; Covance, Princeton, NJ, USA), monoclonal anti-RIP (1:5; Developmental Studies Hybridoma Bank, Iowa City, IA, USA), monoclonal mouse anti-GFAP (1:100; Cell Signaling, Boston, MA, USA), and monoclonal mouse anti-nestin (1:10; Developmental Studies Hybridoma Bank). Each of these antibodies identified neurons, oligodendrocytes, astrocytes, and progenitor specific intermediate filament proteins, respectively. Next the samples were washed 3 times in PBS (pH = 7.4) for 15 min each and then incubated with secondary goat anti-mouse IgG Alexa-Fluor 546 (1:400; Life Technologies) for 2 h at RT. Samples were again washed 3 times in PBS (pH = 7.4) with 15 min washes and cell nuclei were stained with 10 μM Hoechst 33342 (Life Technologies) for 10 min. Samples were rinsed three times in PBS (pH = 7.4), mounted with Prolong Gold antifade reagent (Life Technologies) and imaged using a fluorescent microscope. Six, 10× images were acquired from each sample with 3−4 coverslips per primary antibody stain. Total cell percentages were determined by quantifying in each image the number of positive cells marked with the antibody of interest compared to the total cell number established from the cell nuclei stain, Hoechst 33342. A confocal microscope, Olympus FV1000, with Olympus Fluoview software (B&B Microscopes Ltd., Pittsburgh, PA, USA) was also used to obtain representative IHC images.

2.6. Statistical Analysis. Significance of angle orientation was determined using JMP 10.0 (JMP, Cary, NC, USA) software by the nonparametric Kruskal−Wallis and Dunn's multiple comparison tests. Single factor ANOVA with Tukey's highly significant difference post hoc test was used to determine significance between cell populations. A p-value <0.05 was considered significant in all cases.

3. RESULTS AND DISCUSSION

3.1. Polymer Channel Fabrication and Characterization. We have shown previously that micropatterned surfaces can be prepared from coumarin polyesters by selective washing of non-cross-linked regions of spin coated polymer films.[27] The coumarin polyesters have an absorption in the range of 280−370 nm with a maximum at 320 nm. The above polyesters are also hydrolytically degradable as shown by the decrease of their number-average molecular weight (M_n) from 11k to 6k when incubated in PBS at 37 °C for a 10 week period. In the current work, we extend the micropatterning capability over a larger area by the use of a digital pattern and a super high pressure mercury lamp (Figure 1B). The single shot area of the DMD based maskless photolithography is limited. However, the ability to dynamically change the pattern allows step-and-stitch processes easily so that a pattern of arbitrary size is split into subpatterns of the single shot size and process subpattern one after another. The accuracy of stitching depends on the mechanical accuracy of the $x-y$ stage. In our present system, it is better than 0.5 μm, which is smaller than the single pixel size of the DMD. A standard photolithography stepper

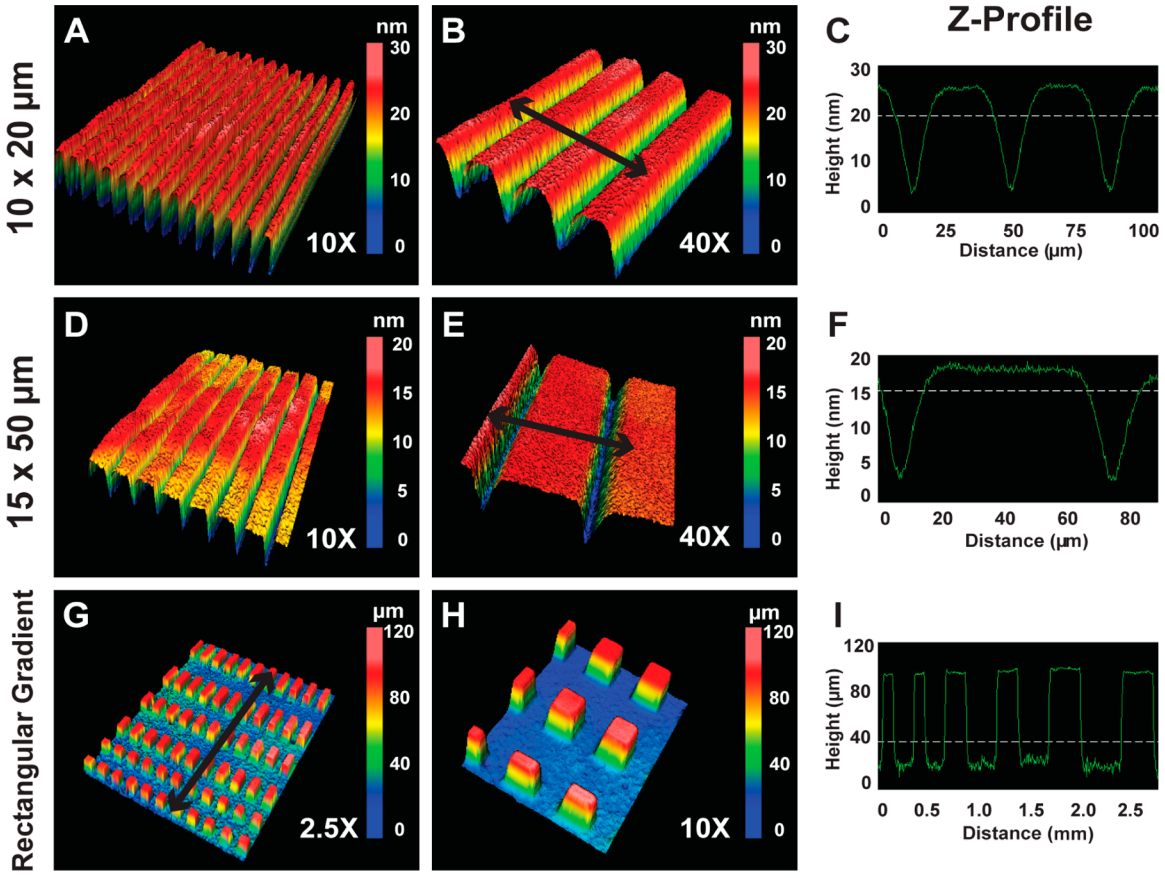

Figure 2. 3D image analysis and measurements of micropatterned channels utilizing optical profilometer. (A) 10 × 20 μm pattern at 10× magnification. (B) 40× magnification of a section of the 10 × 20 μm pattern along with (C) *z*-depth profile at the same magnification showing plateaus and channels with an average depth of 20.1 ± 0.11 nm. (D) 10× image of 15 × 50 μm channels and (E) 40× 3D image of the same channels with the resulting (F) *z*-profile measuring an average depth of 15.8 ± 0.14 nm. (G−H) 2.5× and 10× magnification of a rectangular gradient pattern, respectively. (I) The *z*-profile shows the rectangular gradient with increase in plateau and channel widths. These patterns display the ease and versatility of our DMD maskless patterning system. (B,E,G) Arrows indicate the cross-section for *z*-profiles.

allows normally one inch square area of single shot exposure. To enable a nonperiodic pattern larger than that dimension, one simply needs to make a set of different masks and replace and position the masks each time the step-and-stitch process is carried out.

Microfabrication based on photolithography, which is primarily driving the semiconductor industry, generally consists of a light pattern generator and a projection opto-mechanics. The light patterns are normally generated by metallic photomasks imprinted on glass plates. Preparation of the photomask that faithfully reproduces the designed pattern is one of the most crucial steps in successful microfabrication of complex devices. As the number of photomasks needed for the whole process has increased and the required precision of the photomask has become more stringent, so has a growing demand for a light pattern generator that does not require the photomasks. This new approach of photolithography that does not use conventional photomasks, is referred to as the maskless photolithography. Common to all different types of maskless lithography methods, their advantage becomes most notable in the prototyping and research phase of devices, since the optimization of device patterns can be made with minimum turn-around time and little increase in cost. This feature seems particularly suitable for applications in bioengineering devices that deal with cells and tissues whose behaviors are not as predictable as semiconductor devices.

The maskless lithography system we employed in this study is based on the DMD as the electronically controlled light pattern generator. Specifically, the DMD used in our system consists of independently switchable micromirrors especially developed for maskless lithography applications in the ultraviolet range. According to the digitally created mask pattern fed from a computer, the DMD switches on respective micromirrors. The UV light from an Hg−Xe lamp reflected by the DMD is projected on the sample, usually through demagnifying optics. Our system has two stages in sequence, providing the capability for lower and higher resolution patterning: the first stage gives a 2/3× image of the DMD, providing the finest resolution of coumarin polyester. Ten micrometers over the exposure area of 12 × 7 mm; the second stage gives a 1/10× image, corresponding to the finest resolution of CA11, 1.5 μm over the area of 2.2 × 1.0 mm. The UV light at 365 nm was selected by an interference filter. The intensity at the second stage was 20 mW/cm^2. In addition to the aforementioned advantage of the maskless lithography, our system also has an electronically controlled polarizer so that an arbitrary light pattern not only in terms of the intensity but also in terms of the local polarization is generated. The polarization has a significant impact on the excitation of organic molecules through their anisotropic absorption. The molecular orientation is in fact controllable by the combination of intensity and polarization, which is believed to open up an even

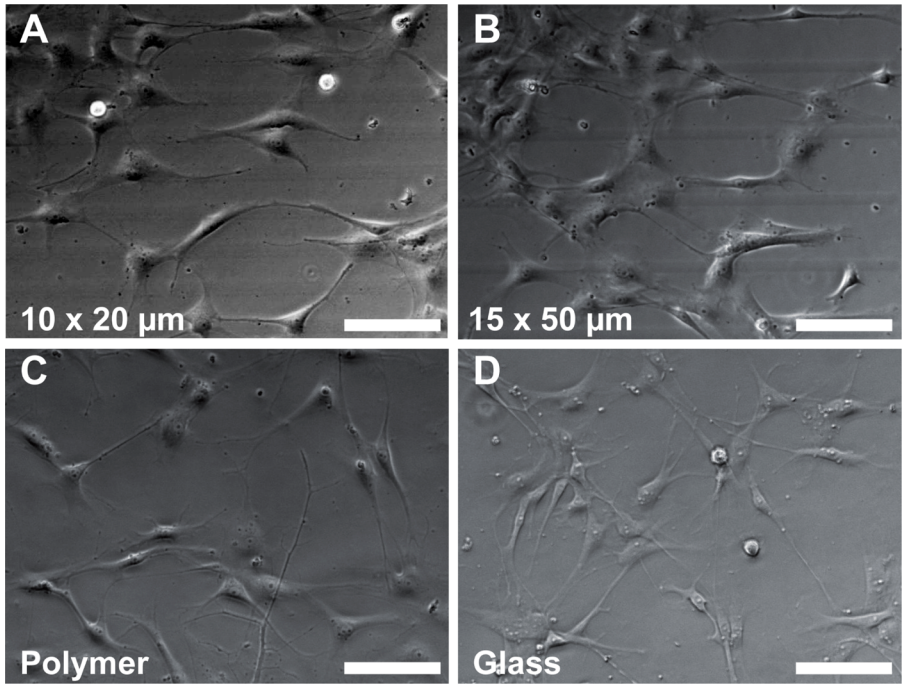

Figure 3. Representative phase contrast images of process alignment for heterogeneous cell population. (A, B) 10 × 20 μm and 15 × 50 μm channels, respectively, display how processes of various cell types align parallel to the channels. In both groups the emergence of the axons from the soma as well as the termination at the growth cone tend to align to the channels. Channels are displayed horizontally as seen in the background of these images. (C, D) Control groups of polymer and glass, respectively, show random neurite outgrowth and extension in an undefined direction. Scale bar =100 μm.

larger control window to achieve optimal cellular environmental conditions.[32−35]

As a result of irradiation at a wavelength of absorption of the coumarin chromophore, the polyester thin films cross-link at regions that are exposed to the irradiation. The unexposed regions can be selectively washed away in a mixture of chloroform−methanol solvent providing a micropatterned surface (Figure 1). The coumarin polyester is soluble in chloroform and insoluble in methanol, while the cross-linked regions are insoluble in both solvents. Therefore, by increasing the ratio of chloroform to methanol in subsequent washes, the nonexposed regions are selectively washed away to produce topographical patterns.

To demonstrate the potential of the technique we micropatterned complex patterns on coumarin polyester thin films. Since the coumarin polyester is fluorescent, the surface patterns can be visualized using a DAPI filter on a fluorescent microscope (Supporting Information Figure S1). These channels along with another pattern were additionally imaged using an IFM. Diverse patterns such as a gradient of rectangles can be patterned very efficiently onto polymer films using the current DMD maskless patterning method (Supporting Information Figure S1). These patterns show the versatility and power of our technique for creating diverse complex micropatterns. However, in this study we focused on simple channel topographies as a proof of concept and guidance model for neurons. Contour maps and depth profiles of these patterns were characterized by optical profilometer measurements (Figure 2). Optical profilometry provides an optimum method for surface characterization when topographical features of the sample range from nanometer to micrometer dimensions. Other techniques such as SEM, IFM or confocal microscopy were not successful in capturing both the nanometer and micrometer sized features. The 10 × 30 μm patterns resulted in 11.0 ± 0.56 μm wide channels, 21.2 ± 0.43 μm wide plateaus, and 20.1 ± 0.11 nm depths (Figure 2A−C). Dimensions for the 10 × 60 μm patterns were 15.8 ± 0.17 μm channels, 47.20 ± 0.25 μm plateaus and a depth of 15.8 ± 0.14 nm (Figure 2D−F). As a result these groups will be referred to their actual measured dimensions (10 × 20 μm and 15 × 50 μm) throughout the remainder of the manuscript. The polymer control coated surface had a roughness root-mean-square (R_{RMS}) value of 1 nm, which is an order of magnitude below the microchannel depths. The rectangular gradient can also be produced with geometries of width and length ranging from 10 to 500 μm and depths on the order of 100 μm (Figure 2G−I).

The methodology utilized here, wherein a maskless patterning technique is used to fabricate micropatterned coumarin polyesters, has several advantages. First, the micropattern is consistent across the entire pattern area resulting in well-defined and smooth channel and plateau geometries (Figure 2). Also the maskless patterning technique enables various features (Figure 2G−I, Supporting Information Figure S1) to be patterned onto the polymer surfaces on a micrometer and nanosized scale (as a step gradient or consistent periodicity) that is relevant for neuronal growth and neurite extension. In addition, the polymer utilized here efficiently undergoes cross-linking upon exposure to wavelengths in the range of 320−365 nm. These polyesters also are advantageous due to their biodegradability, and it is envisioned that the bioresorption rate can be tuned with the regeneration rate of nerve tissue, which we plan to evaluate in longer term experiments. These degradation profiles are an important component of materials that have been used both clinically and in vivo for axonal growth to occur at an optimal rate as well as preventing secondary surgeries needed to remove the NGC

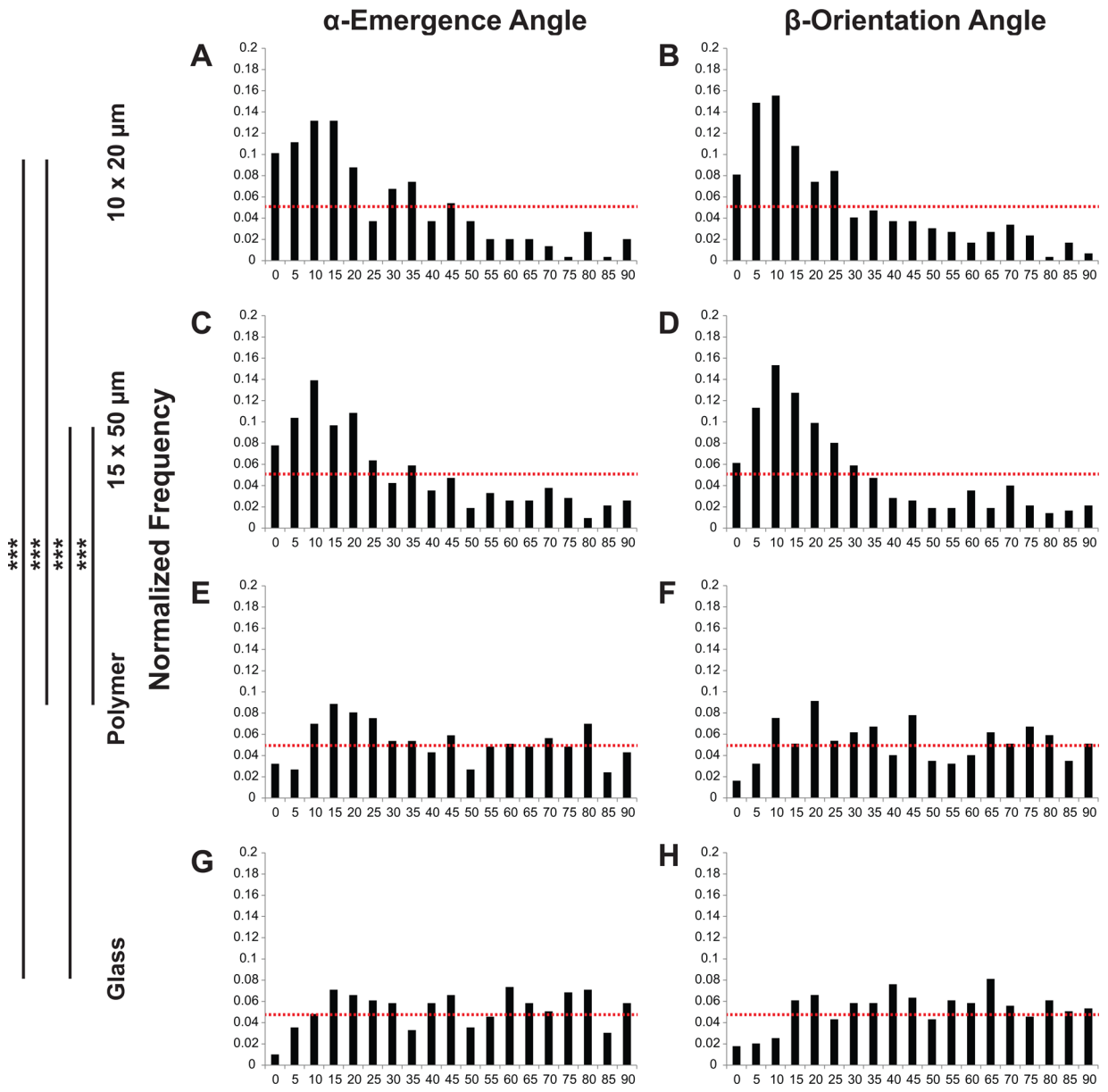

Figure 4. Analysis of neurite emergence and orientation angle alignment. There is no significant difference between α-angle (A, C, E, G) or β-angle (B, D, F, H). The 10 × 20 μm (A, B) and 15 × 50 μm channels (C, D) are statistically difference from both polymer (E, F) and glass (G, H) controls (*** denotes $p < 0.0001$ by the nonparametric Kruskal–Wallis and Dunn's multiple comparison tests). The two channel groups are not statistically different from each other as well as the two control groups. The expected frequency distribution is 0.05 (dashed line). The channel groups (A–D) show a non-normal, parallel distribution where the control groups (E–H) display a more normalized distribution.

(for review, see ref 3). Additionally, our materials platform is tunable and is able to incorporate other guidance cues. These coumarin based polyesters can be functionalized with moieties (such as amines) that allow for specific conjugation of biomolecules.[36] We have recently shown how immobilized guidance proteins are beneficial for sustaining neurite extension and stem cell differentiation.[37−39] Therefore, we could spatially isolate proteins to specific dimensions of the topographies (i.e., ridge, groove, pit, etc.) to enhance and fine-tune the guidance of various CNS or PNS cell populations. There are several materials and patterning methods used for nerve regenerative applications; however, our maskless technique and the polymer used contain multiple characteristics that are optimal for axon guidance platforms.

3.2. Process Alignment to Micropatterned Channels.

Topographical cues are especially important during the initial stages of development where cells begin to polarize into various layers and define their fates.[40] As such contact guidance is applicable to nervous system tissue regeneration where native or delivered cells require specific guidance cues to enable bridging of a damaged or diseased region in the PNS or CNS. Collagen–chitosan NGCs containing microchannels ranging from 25 to 55 μm (geometries similar to the basal lamina of nerves) were formed with a unidirectional freezing method and successfully bridged a 15 mm rat sciatic nerve defect, producing similar regeneration to an autograft control.[41] Our plateau widths (20 and 50 μm) are similar to the endogenous dimensions of nerves, and additionally these plateau and

channel dimensions were specifically chosen since they are also in the range of cell size and axon diameter.[25,26]

Representative phase contrast images from each group after 24 h seeding are shown in Figure 3. From these images it is evident that cells are aligning parallel with both the 10 × 20 μm and 15 × 50 μm channels (Figure 3A−B) compared to the control groups (Figure 3C−D). Cell process angle and alignment are shown in Figure 4 where the emergence angle (α) measured the initial neurite extending from the soma and the orientation angle (β) measured the alignment of the tip of the axon. The controls are more uniformly distributed across the bin range (expected frequency distribution = 0.05) compared to the two channel groups. The 10 × 20 μm and 15 × 50 μm polymer channel groups (Figure 4A−B) were significantly different to both polymer (Figure 4C) and glass (Figure 4D) control surfaces ($p < 0.0001$) for α-angle emergence, but the channels and the control substrates were not significantly different from each other ($p = 0.4815$ and $p = 0.1158$, respectively). Similarly for β-angle alignment, the 10 × 20 μm and 15 × 50 μm channels are both significantly different to the glass and polymer substrates ($p < 0.0001$). Polymer substrates without channels were not significantly different from glass ($p = 0.2672$), and both channels are not significantly different from each other ($p = 1.000$) for β-angle orientation. Processes were considered aligned parallel if they were ≤15° from the horizontal channel/plateau orientation and cell alignment was not designated specifically to either the channel or plateau feature. When analyzing parallel alignment (≤15°) regarding the emergence angle, 10 × 20 and 15 × 50 μm channels exhibited 48% and 42% alignment compared to polymer and glass control, which showed 22% and 17%, respectively. This nonuniformity is also seen in the 10 × 20 μm and 15 × 50 μm groups for the orientation angle (46% and 49%) compared to polymer and glass controls (17% and 12%). For perpendicular alignment of axons ≥75°, percentages were low (5% and 8%) for the emergence angle on 10 × 20 μm and 15 × 50 μm channels compared to 19% for polymer and 23% for glass groups. Orientation angles showed a similar trend with 5% and 7% aligning perpendicularly to 10 × 20 μm and 15 × 50 μm channels whereas 21% of neurites fell within this range for both polymer and glass groups. The expected frequency distribution for parallel or perpendicular alignment of cell processes is 14%, showing that a higher percentage of processes align parallel for both channel groups compared to the polymer and glass control groups which fall around the expected distribution.

The cellular response to our material and patterning technique is comparable to other biomaterials used for neuronal alignment studies. PC12 cells showed 54% and 47% parallel alignment for 1 and 2 μm PLLA channels respectively; however, sympathetic neuron parallel alignment increased to 72% for the 1 μm channels, which has a depth of 150 nm, compared to only 46% for the 2 μm channels with a depth of 215 nm.[31] Our channel dimensions are an order of magnitude larger than these and our depth dimension is much smaller, however, we still achieved statistically relevant cell alignment comparable to what has been observed with PC12 cells. Changes in neuronal alignment has often been observed by varying the channel widths and specific responses of neurite length, number, branching, etc., can be elicited through decreasing the channel width.[23,24] With our study the channel width dimensions were similar at 10 and 15 μm and there was no significant increase in alignment between the 20 and 50 μm plateau groups. Therefore, the lack of significance between groups could be due to this smaller width component being the primary factor driving process alignment. About 70% of astrocytes aligned (≤20°) to PS substrates containing 20 μm wide plateaus and 10 μm wide channels with a depth of 3 μm.[42] Again, about 70% of glial cells aligned parallel (≤10°) to biodegradable poly(D,L-lactide) (PLA) microchannels that were patterned into 20 × 20 μm plateau and channel dimensions with a 3 μm depth using a PDMS mold.[43] Additionally, spiral ganglion neurons achieved over 70% alignment (≤20°) on topographical patterns with 25 μm channel and plateau widths with 7 μm depths.[44] Even though our channel and plateau dimensions are similar to these studies, we did not achieve this high of a percentage of cell process alignment. This is likely due to the different order of magnitude in the depth of the channels.

As discussed previously, decreasing the width of channels is an important factor when designing a guidance platform. However, depth is also an important component in cell orientation studies. It has been shown that increasing this dimension from 200 nm to 4 μm enhances cell alignment percentages and result in an increase in neurite outgrowth and alignment.[18,45−47] Our alignment percentages were not as high as some of the studies reported here, and this could be due to the depths of our channels being between 15 and 20 nm. Interestingly, even with these nanometer-sized depth dimensions, alignment was still achieved. Growth cones of neurites can still sense these minute changes in surface structure even though they are orders of magnitude larger than the topography. Surface roughness ranging from 10 to 100 nm increased hippocampal and cortical neuron adhesion and development.[48] Additionally, an increase in neurite extension was achieved for both PC12 cells and SH-SY5Y human neuroblastoma cells on TiO_2 surfaces with roughness of 20 and 29 nm, compared to glass and TiO_2 films with roughness around 0.25 nm.[49] This is comparable to our study where the surface roughness of the polymer thin films (R_{RMS} = 1 nm) is an order of magnitude smaller than the channel depths. Spiral ganglion neurons displayed the same alignment to 250 nm deep channels with 10 μm frequency from channel to plateau compared to 8 μm depths at 50 μm frequency.[50] This points to the importance of channel width dimensions, but more so to the sensitivity of these neurites to align with these shallow depths orders of magnitude smaller than their physical size. On closer evaluation, one study found that thick filamentous actin (width of 200−500 nm) at the distal end of the growth cone would align to the 350 nm edge of the patterned ridges.[51] As discussed later, we see that processes prefer to anchor to smaller features sizes of our generated micropatterns. There is minimal research studying neuronal and glial response to features less than 20 nm, however, the 10 × 20 μm and 15 × 50 μm channel dimensions proved beneficial in significantly aligning both the emergence and orientation angle of all cellular processes isolated.

Finally, we saw significant alignment between our patterned and control groups even in the presence of laminin adsorption on all groups, pointing to the fact that the topographical features were the main driving force of neurite alignment. As seen in vivo, laminin and neurotrophin distribution and expression is vital for proliferation, differentiation, extension, and migration of neurons.[52,53] It is not surprising to see that when laminin is patterned onto substrates, neurons are guided by and adhere to these geometries.[54−56] Therefore, specifically

incorporating this additional biomolecular component to certain topographical regions would also enhance the overall alignment of our micropattern guidance system. As previously mentioned, these thin film polyesters can be modified in the future to include these additional cues.

3.3. Cell Population and Feature Size Inclination. There was a mixed CNS cell population present after isolation because of oligodendrocytes and astrocytes located in the fractions that were collected. However, the majority of the cells isolated were neurons identified by βIII positive staining as stated below. There is no significant difference between cell-type and substrate based on IHC analysis (Supporting Information Figure S2). Overall the cell population consisted of 71.85 ± 2.4% βIII positive cells (neurons), 4.98 ± 1.1% GFAP expressing cells (astrocytes), 7.82 ± 1.1% RIP positive cells (oligodendrocyte), and 28.42 ± 2.2% cells expressing nestin (progenitor cells). Representative IHC images (Figure 5) show alignment of various cell types on both 10 × 20 μm and 15 × 50 μm channel substrates compared to the control polymer and glass groups (Figure 6).

Approximately 30% of cells expressed nestin in this study. Nestin is an intermediate filament protein marker most commonly associated neural stem and progenitor cells.[57] However, one study showed that nestin expressing cells in the mouse brain also costained for GFAP (astrocyte marker) and goes on to postulate that this dual expression is related to the activation state of the astroglial cells.[58] Comparable to this study, even though we did not costain our cell population, we see morphological components of nestin expressing cells (Figures 5 and 6G, H) that are similar to astrocytes (Figures 5 and 6C, D). Additional cell-based assays would need to further evaluate morphological similarities between astrocytes and nestin expressing cells. However, one reason that we have a higher nestin expressing percentage could be the fact that some of those cells are actually astrocytes. Furthermore, a portion of the nestin expressing cell population could be neural stem and progenitor cells. Topographies have been widely known to not only aid in cell guidance but also in differentiation.[59−61] Since these cells were exposed to the micropatterns for only 24 h, the cells may not have had time to completely differentiate as we typically use longer culture time of 7 days for neural stem cell differentiation studies.[62,63] Since we did not distinguish between cell type in our emergence and orientation angle measurements, we believe that these nestin expressing cells did not affect our alignment percentages. However, it would be interesting to see how longer culture times on these substrates induce differentiation of neural stem and progenitor cells.

Smaller processes of neurons, astrocytes, oligodendrocytes, and nestin expressing cells in general prefer to align or anchor to the plateau/channel interface or along the corner of the channels (Figure 5). On the control substrates, cell process outgrowth did not favor a particular orientation, but cells sent out axons radially in multiple directions (Figure 6B, E, G, H). In this study, no differences were revealed comparing alignment on 10 × 20 μm and 15 × 50 μm channels as process alignment was not separated into alignment to plateaus or channels. However, some cell types aligned better on the narrower 10 × 20 μm topographies compared to the 15 × 50 μm patterns or to the controls (Figures 5 and 6). This was especially evident in the case of oligodendrocytes as they did not spread out as much on the 10 × 20 μm channels (Figure 5E) compared to the 15 × 50 μm channels (Figure 5F). In other research, Schwann cells (myelinating cells of the PNS) isolated from the sciatic nerve

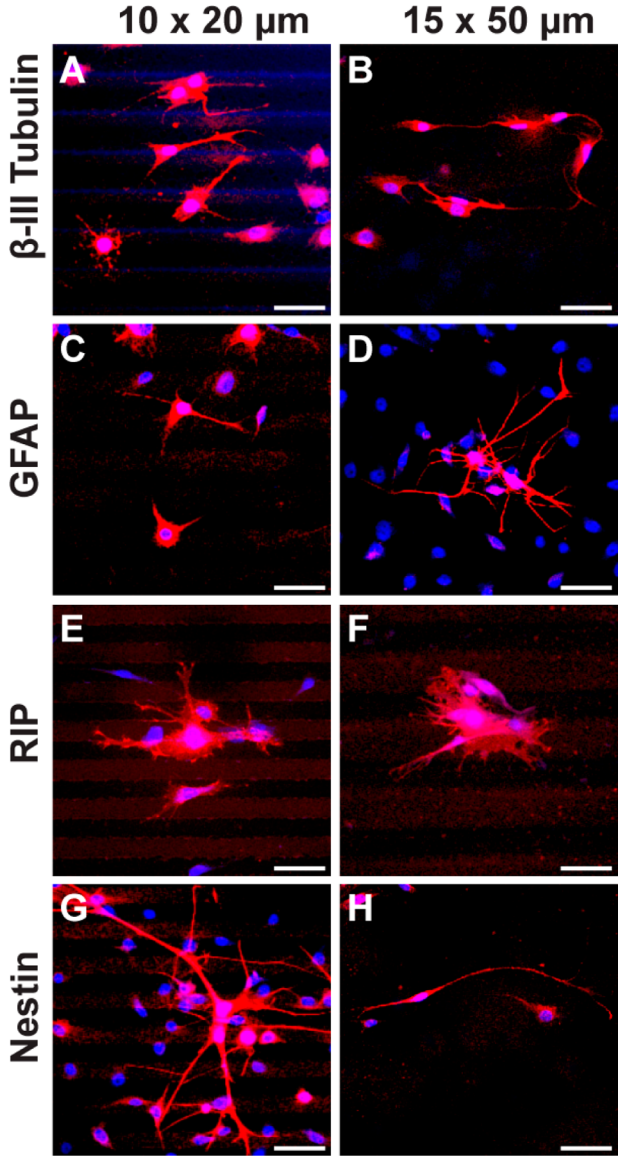

Figure 5. Representative fluorescent images of process alignment on polymer channels. (A, B) Neurons align to 10 × 20 μm and 15 × 50 μm channels respectively with some growth cones anchoring to the corners. (C, D) GFAP expressing astrocytes show some alignment to the channels, especially the smaller processes. (E) Oligodendrocytes show tighter alignment to the 10 × 20 μm channels compared to the 15 × 50 μm channels. (F) Peripheral processes and branches of oligodendrocytes prefer to anchor to the polymer plateaus. (G, H) The smaller branching processes in cells expressing nestin align to both channel groups. Channels are arranged horizontally in the background. Scale bar = 50 μm.

show that 10−20 μm channel widths resulted in the best alignment regardless of depths ranging from about 1.5−3.0 μm.[64] This is comparable to our study where oligodendrocytes (myelinating cells of the CNS) display a difference in cell spreading depending on the plateau even though the channels widths were the same. Alternatively, spiral ganglion Schwann cells, when cocultured with spiral ganglion neurons, significantly increased their alignment when periodicity (channel to plateau) profiles were kept constant but depth measurements increased from 1 to 8 μm.[50] This study in conjunction with other previously mentioned studies shows the importance of all dimensions, width and height of various features, for the

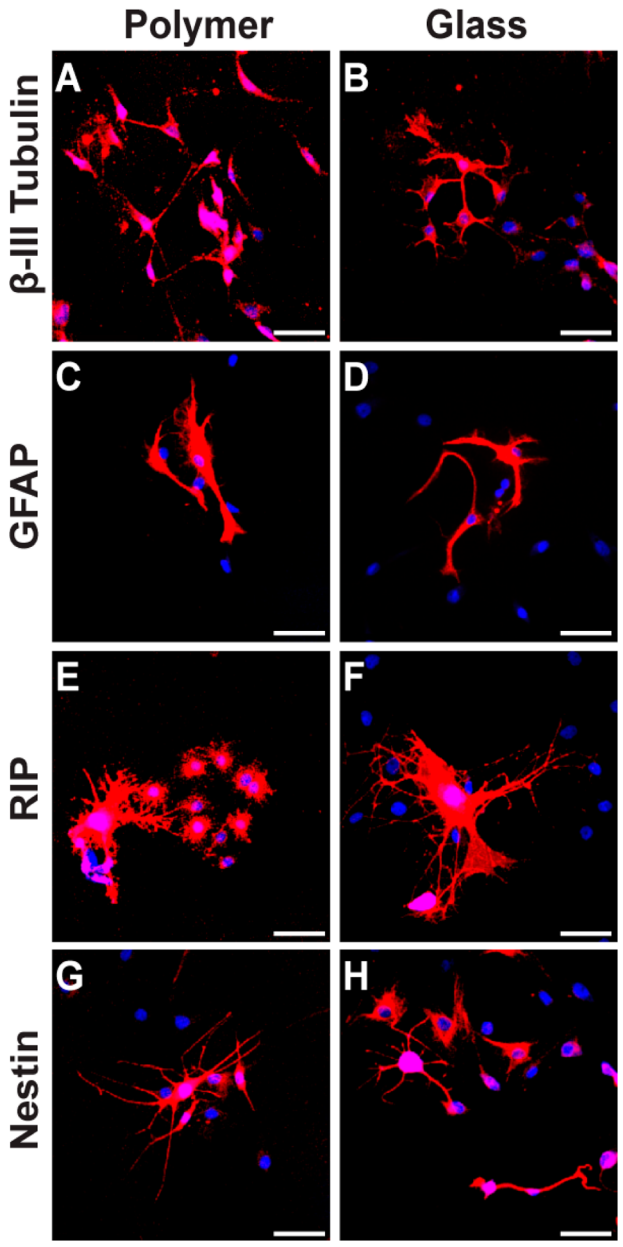

Figure 6. Representative fluorescent images of adult CNS cells on control substrates. Polymer (A, C, E, G) and glass (B, D, F, H) groups show no preference for parallel alignment. Various cell types display more of a radial type of outgrowth (B, E, G, H) where processes search for synaptic targets. Scale bar = 50 μm.

alignment glial cells as well as neurons. Not only did our patterned substrates provide features that were large enough to incorporate the oligodendrocyte somas but we also saw the smaller processes and branches of these cells anchor or begin aligning with the plateau/channel interface (Figure 5E, F). This preference for corners was seen in other larger cell types expressing GFAP and nestin (Figure 5C, D, G, H). Oligodendrocyte and astrocyte processes have been shown to align with 1 μm and submicron features even though the cell bodies are spread over the patterned surface.[65] Astrocytes preferentially aligned their processes to the inside of microchannels or at the plateau/channel boundary when channel widths were reduced from 20 to 10 μm.[42]

Previous studies have also revealed that hippocampal neurons show feature size inclination after 24 h of culture, where axons responded to patterns that were less than 30 μm away, suggesting that this distance is the maximum distance for cell processes to recognize topographical features.[66] Our study agrees with these results as the tip of axons search out these smaller topographies located at the plateau/channel intersection (Figure 5A and B). Other researchers have reported that neurite alignment can be enhanced by decreasing channel widths (1−8 μm depending on cell type) alongside increasing depth.[47,67] Similarly, spiral ganglion neurites showed a significant increase in alignment as the frequency of channel to plateau was reduced from 50 to 10 at 1 μm depths.[50] However, increasing depths to 8 μm, while frequency was widened to 50 μm caused alignment to be similar to shallow 1 μm depths with periodicity at 10 μm.[50] Since alignment was not distinguished to only the plateaus or channels in this experiment, the lack of significance between patterned groups could be due to the fact that the cortical neurons (the smallest and most abundant cell type in the population) preferred to align to the smaller 10 and 15 μm channels in both groups in addition to sensing nanometer-sized depths. This type of selectivity has been seen where certain axons prefer the smaller topographies (300 nm lines and 0.44 μm fibers) over larger patterned features (2 μm lines and 2.2 μm fiber diameter).[66,68] It is important to note that the cell population in this study was heterogeneous, meaning that multiple cell and process sizes were aligning to various features (i.e., plateaus, channels, along the interface) depending on their preference. Most studies focus on pure neuronal populations, however, glia out number neurons to varying degrees in both the native CNS and PNS.[69] We see similar alignment results to studies that have used primary neuronal populations because our isolation techniques selected for a neuronal majority, resulting in about 70% neurons. However, as shown in Figure 5, we do see the other cell types responding and aligning to our micropatterned films. It would be interesting to use this platform as a coculturing system where glial cells (astrocytes and oligodendrocytes) are the majority of the population, and glial-neuronal interactions can be studied and compared to endogenous interactions.[65,70]

Determining the biological mechanism of contact guidance has yet to be fully revealed. It is especially challenging because of the multiple other cues presented to cells that help to shape these responses, as well as the fact that various cell types have preferences for different ranges of topographical sizes that affect their functional and morphological behavior. Recently, several mechanistic hypotheses have been postulated based on previous topographical and cell guidance studies (for reviews, see refs 9 and 71). One common observation is that topographical features directly affect cytoskeletal changes where actin stress fibers and microtubules follow topographical cues minimizing the distortion of the cytoskeleton.[72,73] This phenomenon is seen in neurites as they align parallel with micropatterned substrates.[18,74] In this study, we observed that βIII tubulin positive cells (Figure 5A and B) aligned their axons parallel to the channels and plateaus. It is also commonly accepted that alignment initiated to certain feature of the pattern will induce neurites to follow that particular feature. Hanson et al.[75] noted that hippocampal neurons would continually wrap around PDMS posts with diameters as large as 100 μm when the distances between the posts were greater than 40 μm, but axons would not wrap around posts when distances between the posts were 10 μm. Further investigation

is needed to quantify the topographical feature each cell type favored, whether cells were aligned within the channels or preferred to align to the plateaus.

Not only do topographical geometries affect cellular structure, it also has been shown to change cellular function as well. Integrins are one of the primary pathways that neurons use to connect their cytoskeleton to the extracellular matrix which in turn transduces mechanical stress through these proteins to the cell nucleus through a process known as mechanotranduction.[71,76] Focal adhesion complexes are important structures during mechanosensing as well as cell process outgrowth.[77] Specific to contact guidance, focal adhesions are shown to form along specific geometries.[72,78] Additionally, most focal contacts in certain cell types were located on plateaus compared to channels.[78,79] Along with the notion that cells are inclined to choose smaller features as discussed above, smaller processes (Figure 5) could be anchoring or aligning to the plateaus because the local distribution of focal adhesion complexes is greater in these regions.

4. CONCLUSION

Herein, we demonstrate a unique and efficient technique that leverages the photochemistry of coumarin polyesters for fabricating micron and nanometer scale topographies, which are shown to influence the alignment of a heterogeneous cell population obtained from the rat CNS. Our polymer patterning method is distinctive in that it uses a maskless digital patterning technique in order to fabricate micropatterned channels and can further be used to pattern other geometries through the manipulation of a micromirror device. We show that adult CNS cells (neuronal majority) respond and align parallel to this novel biodegradable polymer with feature sizes of 10 or 15 μm wide channels with either 20 or 50 μm wide plateaus and depths 15 to 20 nm. Control groups do not initiate alignment of cells as processes are normally distributed on the substrates. Immunohistochemical analysis revealed that smaller cell processes align and prefer to anchor to the plateau/channel interface. Overall, these results are encouraging as a first step toward applying this patterned polymer approach to facilitate axon guidance and regeneration after nervous system injury or disease, where quick alignment, host tissue integration, and finally degradation of the material is the preferred approach.

■ ASSOCIATED CONTENT

Supporting Information

2D fluorescent and infinite focus microscopy (IFM) images of micropatterned films, nervous system cell population of β-III tubulin, GFAP, RIP, and nestin positive cells on each substrate prepared for this study. This material is available free of charge via the Internet at http://pubs.acs.org.

■ AUTHOR INFORMATION

Corresponding Authors

*E-mail: abraham@uakron.edu. Telephone: 330-972-6004.
*E-mail: nl21@uakron.edu. Telephone: 330-972-6881.

Notes

The authors declare no competing financial interest.

■ ACKNOWLEDGMENTS

We are grateful to the University of Akron for the funding that supported this work, including the Robert Iredell Endowment to Dr. Nic Leipzig. We would like to thank Dr. Joe Payer and his graduate student Paul Young for their assistance in using the IFM. We are also grateful to Dr. Ina Martin at the MORE Center (Materials for Opto/electronic Research and Education) in the Department of Physics at Case Western Reserve University for the use of the optical profilometer.

■ REFERENCES

(1) Stoll, G.; Muller, H. W. Nerve Injury, Axonal Degeneration and Neural Regeneration: Basic Insights. *Brain Pathol.* **1999**, *9*, 313−25.
(2) Siemionow, M.; Bozkurt, M.; Zor, F. Regeneration and Repair of Peripheral Nerves with Different Biomaterials: Review. *Microsurgery* **2010**, *30*, 574−88.
(3) Nectow, A. R.; Marra, K. G.; Kaplan, D. L. Biomaterials for the Development of Peripheral Nerve Guidance Conduits. *Tissue Eng. Part B Rev.* **2012**, *18*, 40−50.
(4) Wilkinson, A. E.; McCormick, A. M.; Leipzig, N. D. *Central Nervous System Tissue Engineering: Current Considerations and Strategies*; Synthesis Lectures on Tissue Engineering; Athanasiou, K. A., Leach, J. K., Eds.; Morgan and Claypool Publishers: San Rafael, CA, 2011; Vol. 3, p 120.
(5) Chen, B. K.; Knight, A. M.; Madigan, N. N.; Gross, L.; Dadsetan, M.; Nesbitt, J. J.; Rooney, G. E.; Currier, B. L.; Yaszemski, M. J.; Spinner, R. J.; Windebank, A. J. Comparison of Polymer Scaffolds in Rat Spinal Cord: A Step toward Quantitative Assessment of Combinatorial Approaches to Spinal Cord Repair. *Biomaterials* **2011**, *32*, 8077−86.
(6) McCreedy, D. A.; Sakiyama-Elbert, S. E. Combination Therapies in the CNS: Engineering the Environment. *Neurosci. Lett.* **2012**, *519*, 115−21.
(7) McCormick, A. M.; Leipzig, N. D. Neural Regenerative Strategies Incorporating Biomolecular Axon Guidance Signals. *Ann. Biomed Eng.* **2012**, *40*, 578−97.
(8) Zhao, M.; Chalmers, L.; Cao, L.; Vieira, A. C.; Mannis, M.; Reid, B. Electrical Signaling in Control of Ocular Cell Behaviors. *Prog. Retinal Eye Res.* **2012**, *31*, 65−88.
(9) Hoffman-Kim, D.; Mitchel, J. A.; Bellamkonda, R. V. Topography, Cell Response, and Nerve Regeneration. *Annu. Rev. Biomed Eng.* **2010**, *12*, 203−31.
(10) Smith, D. H. Stretch Growth of Integrated Axon Tracts: Extremes and Exploitations. *Prog. Neurobiol.* **2009**, *89*, 231−9.
(11) Silver, J.; Sidman, R. L. A Mechanism for the Guidance and Topographic Patterning of Retinal Ganglion Cell Axons. *J. Comp. Neurol* **1980**, *189*, 101−11.
(12) Krayanek, S.; Goldberg, S. Oriented Extracellular Channels and Axonal Guidance in the Embryonic Chick Retina. *Dev. Biol.* **1981**, *84*, 41−50.
(13) Hatten, M. E. Riding the Glial Monorail: A Common Mechanism for Glial-Guided Neuronal Migration in Different Regions of the Developing Mammalian Brain. *Trends Neurosci.* **1990**, *13*, 179−84.
(14) Harrison, R. G. The Reaction of Embryonic Cells to Solid Structures. *J. Exp. Zool.* **1914**, *17*, 521−544.
(15) Schlosshauer, B.; Dreesmann, L.; Schaller, H. E.; Sinis, N. Synthetic Nerve Guide Implants in Humans: A Comprehensive Survey. *Neurosurg* **2006**, *59*, 740−8.
(16) Rutkowski, G. E.; Miller, C. A.; Jeftinija, S.; Mallapragada, S. K. Synergistic Effects of Micropatterned Biodegradable Conduits and Schwann Cells on Sciatic Nerve Regeneration. *J. Neural Eng.* **2004**, *1*, 151−7.
(17) Miller, C.; Jeftinija, S.; Mallapragada, S. Micropatterned Schwann Cell-Seeded Biodegradable Polymer Substrates Significantly Enhance Neurite Alignment and Outgrowth. *Tissue Eng.* **2001**, *7*, 705−15.
(18) Miller, C.; Jeftinija, S.; Mallapragada, S. Synergistic Effects of Physical and Chemical Guidance Cues on Neurite Alignment and Outgrowth on Biodegradable Polymer Substrates. *Tissue Eng.* **2002**, *8*, 367−78.

(19) de Ruiter, G. C.; Malessy, M. J.; Yaszemski, M. J.; Windebank, A. J.; Spinner, R. J. Designing Ideal Conduits for Peripheral Nerve Repair. *Neurosurg. Focus* **2009**, *26*, E5.
(20) Martinez, E.; Engel, E.; Planell, J. A.; Samitier, J. Effects of Artificial Micro- and Nano-Structured Surfaces on Cell Behaviour. *Ann. Anat.* **2009**, *191*, 126−35.
(21) Nikkhah, M.; Edalat, F.; Manoucheri, S.; Khademhosseini, A. Engineering Microscale Topographies to Control the Cell-Substrate Interface. *Biomaterials* **2012**, *33*, 5230−46.
(22) Le, X.; Poinern, G. E. J.; Ali, N.; Berry, C.; Fawcett, D. Engineering a Biocompatible Scaffold with either Micrometre or Nanometre Scale Surface Topography for Promoting Protein Adsorption and Cellular Response. *Int. J. Biomater.* **2012**, *2013*, 1−16.
(23) Mahoney, M. J.; Chen, R. R.; Tan, J.; Saltzman, W. M. The Influence of Microchannels on Neurite Growth and Architecture. *Biomaterials* **2005**, *26*, 771−8.
(24) Houchin-Ray, T.; Swift, L. A.; Jang, J. H.; Shea, L. D. Patterned PLG Substrates for Localized DNA Delivery and Directed Neurite Extension. *Biomaterials* **2007**, *28*, 2603−11.
(25) Knox, B.; Ladiges, P.; Evans, B. *Biology*; McGraw-Hill: Sydney, Australia, 1994.
(26) Rutten, W. L. Selective Electrical Interfaces with the Nervous System. *Annu. Rev. Biomed Eng.* **2002**, *4*, 407−52.
(27) Maddipatla, M. V. S. N.; Wehrung, D.; Tang, C.; Fan, W.; Oyewumi, M. O.; Miyoshi, T.; Joy, A. Photoresponsive Coumarin Polyesters that Exhibit Cross-Linking and Chain Scission Properties. *Macromolecules* **2013**, *46*, 5133−5140.
(28) Dudley, D.; Duncan, W. M.; Slaughter, J. In *Emerging Digital Micromirror Device (DMD) Applications*; SPIE: San Jose, CA, 2003; pp 14−25.
(29) Blanche, P.-A.; Carothers, D.; Wissinger, J.; Peyghambarian, N. Digital Micromirror Device as a Diffractive Reconfigurable Optical Switch for Telecommunication. *MOEMS* **2013**, *13*, No. 011104.
(30) Brewer, G. J.; Torricelli, J. R. Isolation and Culture of Adult Neurons and Neurospheres. *Nat. Protoc.* **2007**, *2*, 1490−8.
(31) Li, J.; McNally, H.; Shi, R. Enhanced Neurite Alignment on Micro-Patterned Poly-L-Lactic Acid Films. *J. Biomed Mater. Res. A* **2008**, *87*, 392−404.
(32) Tabe, Y.; Yokoyama, H. Two-Dimensional Dynamic Patterns in Illuminated Langmuir Monolayers. *Langmuir* **1995**, *11*, 4609−4613.
(33) Kimura, M.; Nakata, S.; Makita, Y.; Kumano, A.; Takeuchi, Y.; Yokoyama, H. Photo-Rubbing: A General Method to Induce Durable Liquid-Crystal Pretilt Angle on Photo-Alignment Films. *Jpn. J. Appl. Phys.* **2002**, *41*, No. L1345.
(34) Ichimura, K. Photoalignment of Liquid Crystal Systems. *Chem. Rev.* **2000**, *100*, 1847−1874.
(35) Schadt, M.; Seiberle, H.; Schuster, A. Optical Patterning of Multi-Domain Liquid-Crystal Displays with Wide Viewing Angle. *Nature* **1996**, *381*, 212−215.
(36) Chamsaz, E. A.; Sun, S.; Maddipatla, M. V. S. N.; Joy, A. Photoresponsive Polyesters by Incorporation of Alkoxyphenacyl or Coumarin Chromophores along the Backbone. *Photochem. Photobiol. Sci.* **2014**, *13*, 412−421.
(37) McCormick, A. M.; Wijekoon, A.; Leipzig, N. D. Specific Immobilization of Biotinylated Fusion Proteins NGF and Sema3A Utilizing a Photo-Cross-Linkable Diazirine Compound for Controlling Neurite Extension. *Bioconjug Chem.* **2013**, *24*, 1515−26.
(38) Leipzig, N. D.; Wylie, R. G.; Kim, H.; Shoichet, M. S. Differentiation of Neural Stem Cells in Three-Dimensional Growth Factor-Immobilized Chitosan Hydrogel Scaffolds. *Biomaterials* **2011**, *32*, 57−64.
(39) Li, H.; Koenig, A. M.; Sloan, P.; Leipzig, N. D. In Vivo Assessment of Guided Neural Stem Cell Differentiation in Growth Factor Immobilized Chitosan-Based Hydrogel Scaffolds. *Biomaterials* **2014**, *35*, 9049−57.
(40) Edgar, D.; Kenny, S.; Almond, S.; Murray, P. Topography, Stem Cell Behaviour, and Organogenesis. *Pediatr. Surg. Int.* **2004**, *20*, 737−40.
(41) Hu, X.; Huang, J.; Ye, Z.; Xia, L.; Li, M.; Lv, B.; Shen, X.; Luo, Z. A Novel Scaffold with Longitudinally Oriented Microchannels Promotes Peripheral Nerve Regeneration. *Tissue Eng. Part A* **2009**, *15*, 3297−308.
(42) Recknor, J. B.; Recknor, J. C.; Sakaguchi, D. S.; Mallapragada, S. K. Oriented Astroglial Cell Growth on Micropatterned Polystyrene Substrates. *Biomaterials* **2004**, *25*, 2753−67.
(43) Hsu, S. H.; Ni, H. C. Fabrication of the Microgrooved/Microporous Polylactide Substrates as Peripheral Nerve Conduits and In Vivo Evaluation. *Tissue Eng. Part A* **2009**, *15*, 1381−90.
(44) Tuft, B. W.; Xu, L.; White, S. P.; Seline, A. E.; Erwood, A. M.; Hansen, M. R.; Guymon, C. A. Neural Pathfinding on Uni- and Multidirectional Photopolymerized Micropatterns. *ACS Appl. Mater. Interfaces* **2014**, *6*, 11265−76.
(45) Walsh, J. F.; Manwaring, M. E.; Tresco, P. A. Directional Neurite Outgrowth is Enhanced by Engineered Meningeal Cell-Coated Substrates. *Tissue Eng.* **2005**, *11*, 1085−94.
(46) Hirono, T.; Torimitsu, K.; Kawana, A.; Fukuda, J. Recognition of Artificial Microstructures by Sensory Nerve Fibers in Culture. *Brain Res.* **1988**, *446*, 189−94.
(47) Clark, P.; Connolly, P.; Curtis, A. S.; Dow, J. A.; Wilkinson, C. D. Topographical Control of Cell Behaviour: II. Multiple Grooved Substrata. *Development* **1990**, *108*, 635−44.
(48) Wu, Z. R.; Ma, J.; Liu, B. F.; Xu, Q. Y.; Cui, F. Z. Layer-by-Layer Assembly of Polyelectrolyte Films Improving Cytocompatibility to Neural Cells. *J. Biomed Mater. Res. A* **2007**, *81*, 355−62.
(49) Tamplenizza, M.; Lenardi, C.; Maffiolo, E.; Nonnis, S.; Negri, A.; Forti, S.; Sogne, E.; De Astis, S.; Matteoli, M.; Schulte, C.; Milani, P.; Tedeschi, G. Nitric Oxide Synthase Mediates PC12 Differentiation Induced by the Surface Topography of Nanostructured TiO_2. *J. Nanobiotechnology* **2013**, *11*, 35.
(50) Tuft, B. W.; Li, S.; Xu, L.; Clarke, J. C.; White, S. P.; Guymon, B. A.; Perez, K. X.; Hansen, M. R.; Guymon, C. A. Photopolymerized Microfeatures for Directed Spiral Ganglion Neurite and Schwann Cell Growth. *Biomaterials* **2013**, *34*, 42−54.
(51) Jang, K. J.; Kim, M. S.; Feltrin, D.; Jeon, N. L.; Suh, K. Y.; Pertz, O. Two Distinct Filopodia Populations at the Growth Cone Allow to Sense Nanotopographical Extracellular Matrix Cues to Guide Neurite Outgrowth. *PLoS One* **2010**, *5*, e15966.
(52) Rogers, S. L.; Edson, K. J.; Letourneau, P. C.; McLoon, S. C. Distribution of Laminin in the Developing Peripheral Nervous System of the Chick. *Dev. Biol.* **1986**, *113*, 429−35.
(53) Maisonpierre, P. C.; Belluscio, L.; Friedman, B.; Alderson, R. F.; Wiegand, S. J.; Furth, M. E.; Lindsay, R. M.; Yancopoulos, G. D. Nt-3, Bdnf, and NGF in the Developing Rat Nervous System: Parallel as Well as Reciprocal Patterns of Expression. *Neuron* **1990**, *5*, 501−9.
(54) Hammarback, J. A.; McCarthy, J. B.; Palm, S. L.; Furcht, L. T.; Letourneau, P. C. Growth Cone Guidance by Substrate-Bound Laminin Pathways is Correlated with Neuron-to-Pathway Adhesivity. *Dev. Biol.* **1988**, *126*, 29−39.
(55) Clark, P.; Britland, S.; Connolly, P. Growth Cone Guidance and Neuron Morphology on Micropatterned Laminin Surfaces. *J. Cell Sci.* **1993**, *105*, 203−12.
(56) Kam, L.; Shain, W.; Turner, J. N.; Bizios, R. Axonal Outgrowth of Hippocampal Neurons on Micro-Scale Networks of Polylysine-Conjugated Laminin. *Biomaterials* **2001**, *22*, 1049−54.
(57) Namiki, J.; Suzuki, S.; Masuda, T.; Ishihama, Y.; Okano, H. Nestin Protein is Phosphorylated in Adult Neural Stem/Progenitor Cells and Not Endothelial Progenitor Cells. *Stem Cells Int.* **2012**, *2012*, No. 430138.
(58) Chen, L. W.; Hu, H. J.; Liu, H. L.; Yung, K. K.; Chan, Y. S. Identification of Brain-Derived Neurotrophic Factor in Nestin-Expressing Astroglial Cells in the Neostriatum of 1-Methyl-4-Phenyl-1,2,3,6-Tetrahydropyridine-Treated Mice. *Neuroscience* **2004**, *126*, 941−53.
(59) McNamara, L. E.; McMurray, R. J.; Biggs, M. J.; Kantawong, F.; Oreffo, R. O.; Dalby, M. J. Nanotopographical Control of Stem Cell Differentiation. *J. Tissue Eng.* **2010**, *2010*, No. 120623.

(60) Teo, B. K.; Wong, S. T.; Lim, C. K.; Kung, T. Y.; Yap, C. H.; Ramagopal, Y.; Romer, L. H.; Yim, E. K. Nanotopography Modulates Mechanotransduction of Stem Cells and Induces Differentiation through Focal Adhesion Kinase. *ACS Nano* **2013**, *7*, 4785−98.
(61) Fujioka, K.; Hanada, S.; Inoue, Y.; Sato, K.; Hirakuri, K.; Shiraishi, K.; Kanaya, F.; Ikeda, K.; Usui, R.; Yamamoto, K.; Kim, S. U.; Manome, Y. Effects of Silica and Titanium Oxide Particles on a Human Neural Stem Cell Line: Morphology, Mitochondrial Activity, and Gene Expression of Differentiation Markers. *Int. J. Mol. Sci.* **2014**, *15*, 11742−59.
(62) Li, H.; Wijekoon, A.; Leipzig, N. D. 3D Differentiation of Neural Stem Cells in Macroporous Photopolymerizable Hydrogel Scaffolds. *PLoS One* **2012**, *7*, No. e48824.
(63) Leipzig, N. D.; Xu, C.; Zahir, T.; Shoichet, M. S. Functional Immobilization of Interferon-Gamma Induces Neuronal Differentiation of Neural Stem Cells. *J. Biomed Mater. Res. A* **2010**, *93*, 625−33.
(64) Miller, C.; Shanks, H.; Witt, A.; Rutkowski, G.; Mallapragada, S. Oriented Schwann Cell Growth on Micropatterned Biodegradable Polymer Substrates. *Biomaterials* **2001**, *22*, 1263−9.
(65) Webb, A.; Clark, P.; Skepper, J.; Compston, A.; Wood, A. Guidance of Oligodendrocytes and their Progenitors by Substratum Topography. *J. Cell Sci.* **1995**, *108* (Pt 8), 2747−60.
(66) Fozdar, D. Y.; Lee, J. Y.; Schmidt, C. E.; Chen, S. Selective Axonal Growth of Embryonic Hippocampal Neurons According to Topographic Features of Various Sizes and Shapes. *Int. J. Nanomedicine* **2011**, *6*, 45−57.
(67) Rajnicek, A.; Britland, S.; McCaig, C. Contact Guidance of CNS Neurites on Grooved Quartz: Influence of Groove Dimensions, Neuronal Age and Cell Type. *J. Cell Sci.* **1997**, *110*, 2905−13.
(68) Lee, J. Y.; Bashur, C. A.; Gomez, N.; Goldstein, A. S.; Schmidt, C. E. Enhanced Polarization of Embryonic Hippocampal Neurons on Micron Scale Electrospun Fibers. *J. Biomed Mater. Res. A* **2010**, *92*, 1398−406.
(69) Jessen, K. R. Glial Cells. *Int. J. Biochem. Cell Biol.* **2004**, *36*, 1861−7.
(70) Clarke, L. E.; Barres, B. A. Emerging Roles of Astrocytes in Neural Circuit Development. *Nat. Rev. Neurosci* **2013**, *14*, 311−321.
(71) Dalby, M. J. Topographically Induced Direct Cell Mechanotransduction. *Med. Eng. Phys.* **2005**, *27*, 730−42.
(72) Hamilton, D. W.; Oakley, C.; Jaeger, N. A.; Brunette, D. M. Directional Change Produced by Perpendicularly-Oriented Microgrooves is Microtubule-Dependent for Fibroblasts and Epithelium. *Cell Motil. Cytoskeleton* **2009**, *66*, 260−71.
(73) Walboomers, X. F.; Croes, H. J.; Ginsel, L. A.; Jansen, J. A. Growth Behavior of Fibroblasts on Microgrooved Polystyrene. *Biomaterials* **1998**, *19*, 1861−8.
(74) Gomez, N.; Chen, S.; Schmidt, C. E. Polarization of Hippocampal Neurons with Competitive Surface Stimuli: Contact Guidance Cues are preferred over Chemical Ligands. *J. R. Soc. Interface* **2007**, *4*, 223−33.
(75) Hanson, J. N.; Motala, M. J.; Heien, M. L.; Gillette, M.; Sweedler, J.; Nuzzo, R. G. Textural Guidance Cues for Controlling Process Outgrowth of Mammalian Neurons. *Lab Chip* **2009**, *9*, 122−31.
(76) Katsumi, A.; Orr, A. W.; Tzima, E.; Schwartz, M. A. Integrins in Mechanotransduction. *J. Biol. Chem.* **2004**, *279*, 12001−4.
(77) Geiger, B.; Bershadsky, A. Assembly and Mechanosensory Function of Focal Contacts. *Curr. Opin Cell Biol.* **2001**, *13*, 584−92.
(78) Oakley, C.; Brunette, D. M. The Sequence of Alignment of Microtubules, Focal Contacts and Actin Filaments in Fibroblasts Spreading on Smooth and Grooved Titanium Substrata. *J. Cell Sci.* **1993**, *106*, 343−54.
(79) Ohara, P. T.; Buck, R. C. Contact Guidance in Vitro. A Light, Transmission, and Scanning Electron Microscopic Study. *Exp. Cell Res.* **1979**, *121*, 235−49.